Eur Biophys J (1994) 23:239–252

European Biophysics Journal

Fibrin structures during tissue-type plasminogen activator-mediated fibrinolysis studied by laser light scattering: relation to fibrin enhancement of plasminogen activation

R. Bauer [1], S. L. Hansen [1], G. Jones [2], E. Suenson [3]*, S. Thorsen [3], L. Øgendal [1]

[1] Department of Mathematics and Physics, Royal Veterinary and Agricultural University, Thorvaldsensvej 40, DK-1871 Frederiksberg C, Denmark
[2] Daresbury Laboratory, Warrington WA4 4AD, UK
[3] Department of Clinical Biochemistry KB 3-01-1, Rigshospitalet, University of Copenhagen, Blegdamsvej 9, DK-2100 Copenhagen, Denmark

Received: 13 March 1993 / Accepted in revised form: 11 July 1994

Abstract. The aim was to relate fibrin structure and the stimulatory effect of fibrin on plasminogen activation during t-PA-mediated fibrinolysis using Lys^{78}-plasminogen as activator substrate. Structural studies were undertaken by static and dynamic laser light scattering, cryo transmission electron microscopy and by the measurement of conversion of fibrin to X-, Y- and D-fragments. The kinetics of plasmin formation were monitored by measurement of the rate of pNA-release from Val-Leu-Lys-pNA. The process of fibrin formation and degradation comprised three phases. In the first phase, protofibrils with an average length of about 10 times that of fibrinogen were formed. The duration of this phase decreased with increasing t-PA concentration. The second phase was characterized by a sudden elongation and lateral aggregation of fibrin fibers, most pronounced at low levels of t-PA, and by formation of fragment X-polymer. The third phase was dominated by fragmentation of fibers and by formation of Y- and D-fragments. Plasmin degraded the fibers from within, resulting in the formation of long loose bundles, which subsequently disintegrated into thin filaments with a length of less than 10 and a mass per length close to one relative to fibrinogen. Plasmin generation at high t-PA concentrations sets in just prior to (and at low t-PA concentrations shortly after) the onset of the rapid second phase of elongation and lateral aggregation of fibrin fibers. The maximal rate of plasmin formation per mol t-PA was the same at all concentrations of activator and was achieved close to the time of the peak level of fragment X-polymer. Plasmin formation ceased after formation of substantial amounts of Y- and D-fragments. At this stage the length was between 300 and 3 and the mass per length close to 1, both relative to fibrinogen. In conclusion our results indicate that (1) formation of short fibrin protofibrils is the minimal requirement for the onset of the stimulatory effect of fibrin on plasminogen activation by t-PA, (2) formation of fragment X protofibrils is sufficient to induce optimal stimulation of plasminogen activation, and (3) plasmin degrades laterally aggregated fibrin fibers from within, resulting in the conversion of the fibers into long loose bundles, which later disintegrate into thin filaments.

Key words: Biopolymer – Protofibril – Effector function – Fibrin degradation – Rotational diffusion – Dynamic light scattering

Introduction

The t-PA-catalyzed conversion of the proenzyme plasminogen to plasmin and the subsequent plasmin-cleavage of fibrin are considered to play a role in the resolution of fibrin deposits in thrombi and in areas of tissue repair (Thorsen 1992; Wiman and Hamsten 1990). The plasmin degradation of fibrin is a highly specific process. This specificity is related to two main mechanisms. Firstly, t-PA, plasminogen and fibrin form a ternary complex which leads to an enhanced rate of plasmin formation in association with the fibrin surface (Hoylaerts et al. 1982). Secondly, fibrin decreases the rate of t-PA and plasmin inhibition by their specific inhibitors, plasminogen activator inhibitor-1 and α_2-plasmin inhibitor, respectively.

The stimulatory effect of fibrin on plasminogen activation during fibrinolysis is variable, since the precursor, fibrinogen ($M_r = 340\,000$, consisting of two identical disulfide-linked structures, each containing an Aα-, Bβ- and γ-polypeptide chain) and fibrin itself are continuously modified by thrombin- and plasmin-cleavages yielding a diversity of reaction products (Doolittle 1984; Mosesson

The present work has been supported by the Danish Natural Science Research Council and the Danish Agricultural and Veterinary Research Council

* Deceased on August 2, 1991

Abbreviations: t-PA, tissue-type plasminogen activator; Lys^{78}-plasminogen, plasmin-modified plasminogen, mainly with NH_2-terminal lysine (residues 78–791, residue numbering according to Forsgren et al. 1987); Val-Leu-Lys-pNA, H-D-valyl-L-leucyl-L-lysine-4-nitroanilide; Phe-Pip-Arg-pNA, H-D-phenylalanyl-L-arginine-4-nitroanilide; pNA, p-nitroanilide; SDS, sodium dodecyl sulphate

Correspondence to: R. Bauer

1992; Shafer and Higgins 1988). Initially, thrombin catalyzes the release of fibrinopeptide A (residues 1–16) from the NH_2-terminal part of the Aα-chains of fibrinogen. This release exposes an A polymerization site in the central region of the molecule (E domain) which binds to the COOH-terminal region (D domain) of another molecule to form staggered overlapping dimers and oligomers, which subsequently extend to form elongated, thin, two-stranded fibrils (desA-fibrin), also denoted protofibrils. With some delay thrombin catalyzes the release of fibrinopeptide B (residues 1–14), preferentially from the NH_2-terminal part of the Bβ-chain of polymerizing fibrin and evidently exposes an independent B polymerization site. Fibrinopeptide B release promotes lateral association and branching of protofibrils, yielding a three-dimensional network of thick fibers (desAB-fibrin).

Plasmin-catalyzed modification of fibrin involves cleavage of numerous Lys-X and Arg-X bonds (Medved' et al. 1986; Mihalyi 1983; Nossel et al. 1983). The majority of highly labile bonds are in the hydrophilic COOH-terminal protuberances of the (A)α-chains (Lys^{206}-Val^{610}). Cleavage of these bonds leads to the release of parts, or the whole, of one or both COOH-terminal protuberances. The Arg^{42}-Ala^{43} bonds in the NH_2-terminal Bβ-chains of desA-fibrin are also rapidly cleaved by plasmin, releasing the NH_2-terminal residues 1–42 (Nossel et al. 1983). The early plasmin-cleavages lead to formation of a heterogeneous population of X fragments, which are still solid-phase polymers, but containing impaired polymerization sites. More extensive plasmin-cleavage of the α-, β- and γ-chains in the central part of the coiled-coil region splits fragment X-polymer into soluble Y and D fragments and fragment Y into D and E fragments.

The stimulatory effect of fibrin on plasminogen activation requires fibrinopeptide A release from fibrinogen (Suenson and Petersen 1986; Suenson and Thorsen 1988). Evidence exists that formation of fragment X-polymer is necessary for optimal second phase enhancement of plasminogen activation (Norrman et al. 1985; Suenson et al. 1994; Suenson and Thorsen 1988; Suenson et al. 1990). Plasmin-cleavage of fragment X-polymer to Y and D fragment leads to cessation of enhancement of plasminogen activation. Up to now, little is known about size of the polymer structures or the sites which are cleaved by plasmin when optimal fibrin stimulation of plasmin generation sets in or when the stimulatory effect ceases (Kaczmarek et al. 1993; Suenson and Petersen 1986).

The structure of fibrin polymers has been the subject of many studies using static and dynamic light scattering as well as electron microscopy (Carr et al. 1977; Casassa 1955; Hantgan and Hermans 1979; Hunziker et al. 1990; Marx 1988; Medved' et al. 1990; Mueller and Burchard 1978; Palmer and Fritz 1979; Weisel and Nagaswami 1992). The aim of this paper is to present laser light scattering and electron microscopy data on the structural features of fibrin polymers, which are of importance for their stimulatory effect on plasminogen activation by t-PA.

Materials and methods

Reagents

Tris buffer: 50 mM Tris-HCl, 100 nM NaCl, 0.01% (v/v) Tween 80, adjusted with NaOH to pH 7.7 at 25 °C. Phe-Pip-Arg-pNA
(S-2238) and Val-Leu-Lys PNA (S-2251) were from Chromogenix AB (Mölndal, Sweden). Preparations of human fibrinogen, ^{125}I-labeled fibrinogen, thrombin, Lys^{78}-plasminogen and single-chain t-PA were those described (Suenson and Thorsen 1988). Two-chain t-PA was prepared according to Petersen et al. (1987).

Concentration of proteins

The concentrations of Lys^{78}-plasminogen and fibrinogen were determined spectrophotometrically at 280 nm (Thorsen 1975). The concentration of active t-PA was determined by an immunosorbent assay (Petersen et al. 1987). The concentration of thrombin was determined at 25 °C by measuring the initial rate of hydrolysis of Phe-Pip-Arg-pNA (425 μM) in Tris buffer and using the kinetic constants $K_m = 2$ μM and $k_{cat} = 91.4\ s^{-1}$ (Jørgensen et al. 1984).

Assay system and experimental conditions

All experiments were carried out at 25 °C. The system examined contained fibrinogen (150 nM), Lys^{78}-plasminogen (50 nM), Val-Leu-Lys-pNA (600 μM), thrombin (130 pM) and t-PA (0–100 pM) in Tris buffer. Fibrin formation and plasminogen activation were intitiated by simultaneous addition of thrombin and t-PA to the system.

Laser light scattering analysis: dynamic laser light instrumentation

The experimental arrangement consisted of a 35 mW HeNe laser, Spectra Physics model 127 and an ALV5000 multiple tau autocorrelator on a single expansion board in a Personal Computer for experimental control and data collection. The detector was a red sensitive photomultiplier tube, Hamamatsu R649 in combination with a photon counting unit, Hamamatsu C1050. A computer controlled attenuation system was built to adjust the power incident on the sample. This was necessitated by the fact that light scattering power of the sample (the Rayleigh ratio) increased by several orders of magnitude during polymerization and the fact that too high scattering intensity would overload the detecting system. The automatic attenuation system consisted of a facility to monitor the count rate of the detecting system and a variable circular attenuator, (Newport 50G00AV.2) with a transmission coefficient varying continuously from 0.01 to 1, driven by a stepper motor. Prior to each measurement the count rate of the detector was read and the

computer automatically would adjust the attenuation accordingly. The resulting magnitude of the laser power was stored in a separate log file to be used during data analysis (Eq. (4) below).

Analysis of the dynamic light scattering spectra

The aim of the analysis of dynamic light scattering spectra is to obtain a distribution of relaxation times present in the sample. Since the photon count rate is also measured and stored in the correlation spectrum file it is possible to determine the Rayleigh ratio of the sample. No universally accepted single method to analyze autocorrelation functions exists. The reason is that the analysis is mathematically equivalent to an inverse Laplace transform on noisy data. This is known to produce an infinite number of possible solutions unless constraints are imposed. Using the program CONTIN (Provencher (1982), adapted by the ALV company) gave very broad distributions of relaxation times which would have to be interpreted in terms of translational and rotational diffusion coefficients. However, to produce unambiguous results CONTIN generally requires very good quality data which were not obtainable in this study because the measurement time of each spectrum was limited to 20 s in order to obtain proper time resolution. The measured homodyne autocorrelation function can in general be written

$$g^{(2)}(t) = C_{\text{coh}}(g^{(1)}(t))^2 + 1 \tag{1}$$

where t is the correlation time and C_{coh} is the spatial coherence factor (an instrumental constant). The mathematical form of $g^{(1)}(t)$ depends on the physical properties of the system investigated. In the present case it was necessary to employ different functional forms of $g^{(1)}(t)$ depending on the state of the system (i.e. how far the polymerization and subsequent degradation had proceeded). We employ the form of $g^{(1)}(t)$ shown in Eq. (2) to describe both gel relaxation and free translational diffusion of a polydisperse system whereas we employ the form of $g^{(1)}(t)$ shown in Eq. (9) to describe a system where both translational and rotational diffusion contribute significantly to the measured correlation function.

In the phases where rotational diffusion could be neglected the least squares fitting to the autocorrelation spectra employed the following expression for $g^{(1)}(t)$

$$g^{(1)}(t) = A_1 e^{-(D_1^* q^2 t)^\beta} + A_2 e^{-\Gamma_2 t} \tag{2}$$

where A_1 and A_2 are positive amplitude factors satisfying $A_1 + A_2 = 1$, β is a fitting parameter introduced to account for a polydisperse distribution of molecules (Patterson, 1983), D_1^* is a diffusion coefficient parameter, Γ_2 is a relaxation constant fixed to 0.1 s^{-1} and q is the length of the scattering vector given by

$$q = \frac{4\pi n}{\lambda_0} \sin\frac{\theta}{2} \tag{3}$$

where n is the refractive index of the sample solution, λ_0 is the vacuum wavelength of the laser beam and θ is the scattering angle of the light. The amplitude A_1 is proportional to the Rayleigh ratio of the species to which it pertains. This means that

$$M_1 C_1 P_1(q) = K A_1 \frac{n_{\text{phot}}}{P_{\text{laser}}} \sin\theta \tag{4}$$

where $P_1(q)$ is the form factor of the molecular species with molar mass M_1 and weight concentration C_1, P_{laser} is the measured laser power, n_{phot} is the measured mean photon count rate, and K is an instrumental constant which has been determined empirically using yeast superoxide dismutase as a calibrating standard. The term $\sin\theta$ corrects for the change in scattering volume with detector angle. In the absence of concentration effects $M_1 P_1(q)$ can be regarded as the *apparent molar mass*. The constant K was subsequently found to give the correct molar masses of carbonic anhydrase (3.0 g/L), bovine serum albumin (1.0 g/L) and human fibrinogen (0.05 g/L). The second exponential term in Eq. (2) is included in order to be able to allow for trace amounts of impurities (dust and aggregated protein) of very large size in the sample (and to correct for very slow decays for which the data collection time is too short. These might be present owing to the nonergodic nature of the gelling system. The relaxation constant is fixed to avoid values interfering with the first term in Eq. (2)). These impurities will also contribute to the total light scattering of the sample even if their weight concentration is small, because light scattering scales as the weight concentration times the mass. If the molar mass of the impurities is sufficiently high (which is indicated by their corresponding low diffusion coefficient, i.e. low value of Γ_2) then their possible contribution to the total weight concentration can be neglected. In Eq. (2) the range of β is 0 to 1 where $\beta = 1$ corresponds to an infinitely sharp distribution and $\beta = 0$ to an infinitely wide distribution of diffusion coefficients. A measure of the polydispersity is then suggested to be $(1-\beta)/\beta$. When $\beta < 1$ the distribution is no longer symmetrical and the value for the mean diffusion coefficient is different from the fitting parameter D_1^* in Eq. (2). The mean value of the distribution of the inverse diffusion coefficients $\langle 1/D_1 \rangle$ belonging to species of class 1 is given by Patterson (1983)

$$\langle 1/D_1 \rangle = \frac{\Gamma(1/\beta)}{D_1^* \beta} \tag{5}$$

where Γ is the gamma function. We then define the average diffusion coefficient to be $1/\langle 1/D_1 \rangle$.

Models for the apparent molar mass and average diffusion coefficient

In order to derive information about the structures of protofibrils, gel and plasmin digested fragments from the apparent molar mass and average diffusion coefficient it is necessary to use a model for the structure to fit the two measured quantities. Electron microscopy (Carr et al. 1977; Casassa 1955; Medved et al. 1990) has shown that very elongated molecules are dominant during all stages of the fibrin polymerization. We have therefore modelled the molecules as rigid cylinders with length L and radius

R. The molar mass is then given by

$$M_1 = N_A(\varrho\,\pi R^2 L) \tag{6}$$

where N_A is Avogadro's number and ϱ is the mass density. The form factor for the cylinder was calculated using the semianalytical formula (Feigin and Svergun 1987)

$$P(q) = 4\int_0^1 \left(\frac{J_1(qR(1-x^2)^{1/2})}{qR(1-x^2)^{1/2}} F(qLx/2)\right)^2 \mathrm{d}x \tag{7}$$

where $F(t) = \sin(t)/t$ and $J_1(t)$ is the Bessel function of the first kind of order 1.

This diffusion coefficient for a single cylindrical species was calculated as described by Richards (1980)

$$D = \frac{2kT\left(\frac{1}{2}p - \ln p + 0.577\right)}{6\pi\eta L} \tag{8}$$

where k is Boltzmann's constant, T is the absolute temperature, $p = 2R/L$ is the axial ratio and η is the viscosity of the solvent at temperature T.

The use of an autocorrelation function of the form given in Eq. (2) with the parameters A_1 and D_1^* given by the cylinder model requires that the cylinders are non-rotating. This seems to be a reasonable assumption in the gel phase because cross links will inhibit free rotation. (The possible effect of branching on light scattering is not considered in this model but is supposedly small owing to the long linear stretches between cross links (Wachenfeld-Eisele and Burchard 1988)). Moreover, the use of an autocorrelation function of the form of Eq. (2) is necessary in the gel phase owing to the large apparent polydispersity. In the phase of plasmin degradation molecules short enough to rotate freely will ultimately be produced. However, they are not likely to be rigid cylinders and more importantly they are expected to represent a broad distribution of differently sized molecules which justifies the use of Eq. (2). But in the lag phase polydispersity is low and the oligomers are adequately modelled as elongated freely rotating rigid cylinders, so in this phase rotational diffusion must be included. An expression for the autocorrelation function for freely rotating rigid cylinders for arbitrary values of the length of the scattering vector, q, relative to the length, L, of the cylinder is given by Schmitz (1990) (see also Russo 1993):

$$g^{(1)}(t) = A\,e^{-D_1 q^2 t}\sum_{j=0}^{\infty}(2j+1)\,B_j(qL)\,e^{-j(j+1)D_\theta t} \tag{9}$$

where A is a normalization constant, B_j is a sum of Bessel functions as described in Schmitz (1990) and D_θ is the rotational diffusion coefficient given by

$$D_\theta = \frac{3kT(\ln(p)+\gamma)}{\pi\eta L^3} \tag{10}$$

where $\gamma = -0.662 + 0.917/p - 0.050/p^2$. In Eq. (9) the translational diffusion coefficient D_1 changes gradually from $D_1 = D$ (given by Eq. (8)) when $qL \approx 1$ to $D_1 = 0.75\,D$ when $qL = 40$ (Russo 1993).

Fitting of autocorrelation spectra from the first phase of fibrinogen polymerization

It is necessary to know the weight concentration (C_1) of polymerized fibers in order to calculate the apparent molar mass (M_1) from Eq. (4). This value can be considered to be equal to the initial weight concentration of fibrinogen at late stages of fibrin formation. However, during the slow first phase of fibrin polymerization (Ending after 700–1500 s; Figs. 4 and 6) it was calculated that thrombin (130 pM) converted only 40–65% of the fibrinogen to desA-fibrin, when it was assumed that k_{cat}/K_m (25 °C) is two fold lower than k_{cat}/K_m (37 °C) $= 1.09 \cdot 10^7\ \mathrm{M^{-1}\,s^{-1}}$ for the thrombin-catalyzed release of fibrinopeptide A (Lewis et al. 1985). This gives $T_{1/2} = 980$ s, in agreement with experimental data of Blombäck and Okada (1982) and Wiltzius et al. (1982). In order to correct for the presence of fibrinogen during the first phase of fibrin polymerization the length and mass per length of fibrin oligomers are derived from the light scattering data using a sum of three terms for $g^{(1)}(t)$: The oligomers are represented by the term given in Eq. (9) for cylinders including rotational diffusion, fibrinogen is represented by an exponential term with an exponent containing the known diffusion coefficient for fibrinogen and an amplitude calculated from the time dependent weight concentration and $M_r = 340\,000$. The third term is the usual "dust term" with a fixed relaxation constant:

$$g^{(1)}(t) = A_1\,e^{-D_1 q^2 t}\sum_{j=0}^{\infty}(2j+1)\,B_j(qL)\,e^{-j(j+1)D_\theta t} + A_3\,e^{-\Gamma_3 t}. \tag{11}$$

This procedure resulted in satisfactory χ^2 values in the first phase i.e. for lengths less than 20 times that of the monomer (Fig. 5).

Fitting of autocorrelation spectra from the second and third phase of fibrinogen polymerization

As mentioned, the autocorrelation function including rotational diffusion is only meaningful up to a certain length of the cylinder (for a given concentration of protein) because free rotation of the individual cylinders is eventually hindered by their neighbors (Maguire 1981). This restricts the use of Eq. (11) to the first phase. Fitting the autocorrelation spectra using Eq. (1) with the theoretical function given in Eq. (2) should, as previously argued, be restricted to the second and third phase. However, it was also chosen to fit the autocorrelation spectra from the first phase in this way in order to obtain the amplitude A_1, the average diffusion coefficient $1/(1/\langle D_1\rangle)$ and the polydispersity (through the value of β) in a uniform way for the entire time course. Results are shown in Figs. 1 and 5. Finally, using Eqs. (4)–(8) the radius and length of the cylinder are obtained. To obtain agreement with the measured diffusion coefficient for fibrinogen equal to $0.21 \cdot 10^{-10}\ \mathrm{m^2\,s^{-1}}$ at 20 °C (Van der Drift et al. 1983) a cylinder of 46 nm long and 3.4 nm in cross sectional diameter with a hydration layer of 2.6 nm was used giving a diameter of 8.6 nm. The values for the hydrated

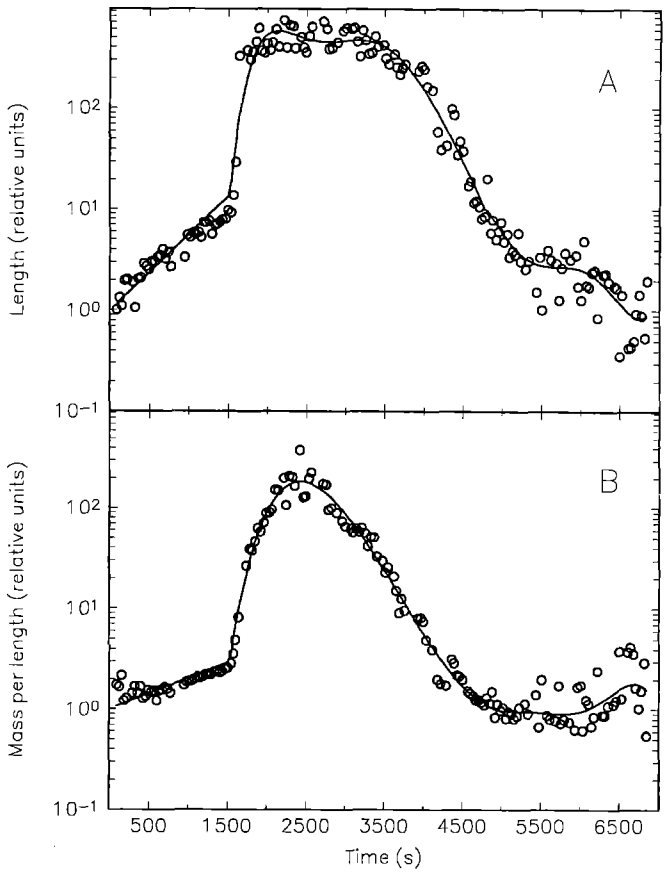

Fig. 1. Polynomial fits (*solid curves*) to data (*circles*) for relative length **A** and relative mass per length **B** of fibrin fibers versus time during thrombin induced polymerization and single-chain t-PA-mediated fibrinolysis. The data for relative length and relative mass per length were obtained via the cylinder model and fitting of the autocorrelation functions using Eqs. (1) and (2) throughout the time course. Fibrinogen (150 nM), Lys^{78}-plasminogen (50 nM) and Val-Leu-Lys-pNA (600 μM) in Tris buffer were incubated at 25 °C in a thermostated cuvette. Fibrin formation and plasminogen activation were initiated by simultaneous addition of thrombin (130 pM) at t-PA (3 pM) in the same buffer. Length (panel A) and mass per length (panel B) are both given relative to fibrinogen. The logarithms of values for length or mass per length versus time (obtained at 30 s intervals) were fitted with polynomials. This was done after dividing the time course into three sections (0–1600 s, 1600–4800 s and after 4800 s) with overlapping regions (plus/minus 5 spectra equivalent to 150 s). The data points in the early slow first phase of fibrin assembly were fitted with a first order polynomial while the data points in the two following sections were fitted with 6th to 10th order polynomials. For further details see Materials and methods

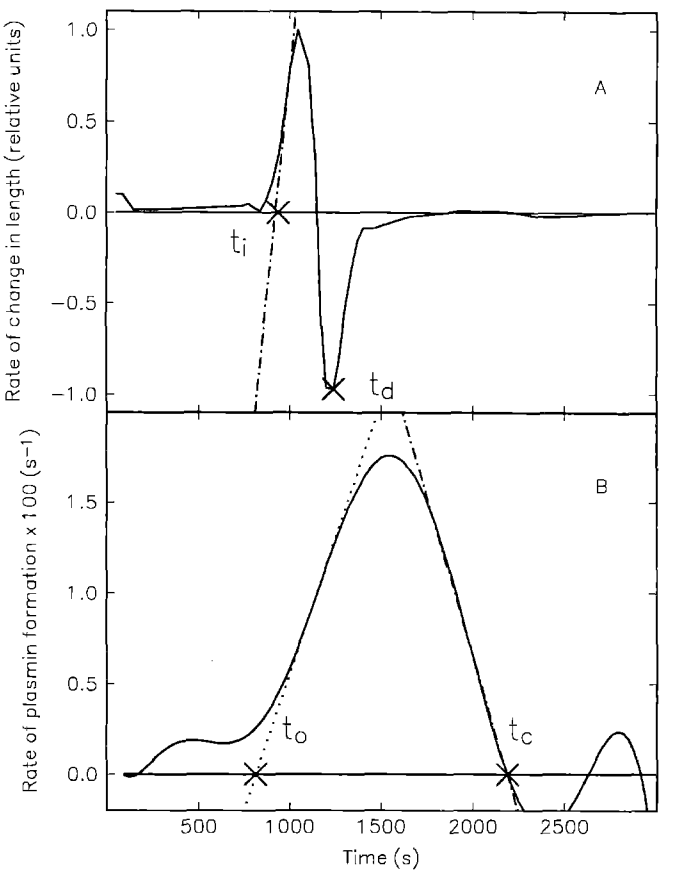

Fig. 2. Definition of specific times for length (light scattering) and plasmin generation. Panel A shows the first order derivative of time course of length shown in Fig. 4D. The derivative curve was arbitrarily normalized to have a maximum value of 1. It was used to define the onset time of sudden increase (t_i) and the time of maximal rate of decrease (t_d) in length. The time t_i is the intercept between the time axis and the tangent at the half maximum point before the maximum of the derivative plots and t_d is the time of the minimum of the derivative plots. The t_i and t_d values for mass per length and turbidity, respectively, were defined in the same way (see Materials and methods). Panel B shows the first order derivative of the plasmin generation curve in Fig. 8 (*upper panel*). This derivative curve reflecting the first order rate of plasmin formation versus time was used to define the onset time of plasmin generation (t_0) and the cessation time of plasmin generation (t_c) which were the intercept between the time axis and the tangent at the half maximum before and after the maximum rate of plasmin formation, respectively

and dry volume thus obtained are in agreement with published values (Van der Drift et al. 1983; Montejo et al. 1992). This hydration was used in the least squares fits at all stages of the polymerization and degradation of fibrin. The hydration can be converted to an equivalent mass density of 0.12 g cm^{-3} whereby the mass per length is derived.

In order to reduce noise fluctuations between consecutive values (obtained at 30 s intervals) of the length or mass per length so that a meaningful time derivative of the value could be made and in order to ensure maximal curve continuity the logarithm of the length or mass per length data as a function time were fitted with polynomials. This was done after dividing the time course into three sections with overlapping regions (plus/minus 5 spectra equivalent to 150 s). An example of a data fit is shown in Fig. 1. The data points in the early slow phase of fibrin polymerization were fitted with a first order polynomial while the data points in the two following sections were fitted with 6th to 10th order polynomials. The values of length or mass per length versus time were transformed to produce derivative plots ($\Delta s/\Delta t$ versus time (t_m)) normalized to have a maximal value of $\Delta s/\Delta t = 1$; Δs is the change in length or mass per length over the fixed time interval $\Delta t = t_2 - t_1$ ($= 30$ s) and $t_m = (t_1 + t_2)/2$. These derivative plots were used to define the

onset time of sudden increase (t_i) and the time of maximal rate of decrease (t_d) in either length or mass per length (Fig. 2A). The time t_i is the intercept between the time axis and the tangent at the half maximum point before the maximum in the derivative plots and t_d is the time of the minimum in the derivative plots.

Cryo transmission electron microscopy

The time course of fibrin polymerization and degradation was followed by cryo electron microscopy by withdrawing 10 µl of the reaction solution at given times after addition of thrombin and t-PA. The samples withdrawn were then immediately placed on a "holey" carbon grid and rapidly immersed in liquid ethane. The cryo transfer system (Gaton model 626, Pleasanton, CA, USA) was used to transfer the specimen to a Philips EM 400 electron microscope fitted with a minimum dose kit. Images taken at magnification 46k were recorded on film S0163 (Eastman Kodak Co).

Assay of plasminogen activation kinetics and change in fibrin turbidity during t-PA-mediated fibrinolysis

The time course of plasmin generated from plasminogen activated by t-PA and change in fibrin turbidity were measured simultaneously with 30 s intervals by a HP model 8452A diode array spectrophotometer (Hewlett Packard, Rockville, MD, USA) or a Shimadzu 60 spectrophotometer, selecting the wavelengths 404, 434 and 474 nm (Suenson and Petersen 1986). The amount of plasmin formed was calculated from the rate of release of pNA from Val-Leu-Lys-pNA. Formation of pNA was recorded at two different wavelengths (404 and 434 nm) and the amount of pNA at any given time was calculated from the absorbance difference $A_{404-434}$ using the extinction, coefficient, $\varepsilon_{404-434}=7165\ M^{-1}\ cm^{-1}$. This was done in order to minimize the influence of fibrin (derivative) turbidity. The low amounts of plasmin generated at 3–13 pM t-PA made it necessary to subtract the turbidimetric contribution of fibrin(derivative) to $A_{404-434}$. The value to be subtracted was calculated by multiplying the absorbance at 474 nm (assumed to originate solely from light scattering) with a factor equal to $(474/404)^3-(474/434)^3$. The validity of this correction procedure is based upon a λ^{-3} dependency of turbidity of fibrin derived from other studies (see for example Carr et al. 1977, Hantgan and Hermans 1979). Data for number of moles plasmin formed per mol t-PA versus time were fitted with 6th to 10th order polynomials (Fig. 8, upper panels). The same data were used to construct derivative plots reflecting the rate of plasmin formation ($\Delta p/\Delta t$) per mol t-PA versus time (t_m), where Δp is the increase in amount of plasmin over the fixed time interval $\Delta t=t_2-t_1$ ($=30$ s) and $t_m=(t_1+t_2)/2$. These derivative plots were used to define the onset time of plasmin generation and the cessation time of plasmin generation which were the intercept between the time axis and the tangent at the half maximum before and after the maximum rate

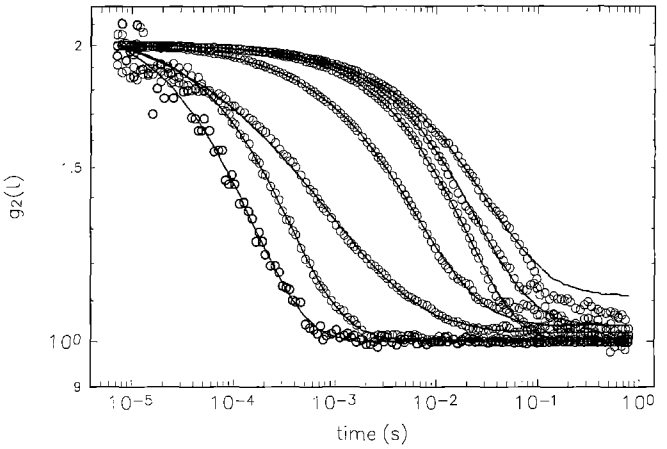

Fig. 3. Experimental (*circles*) autocorrelation functions $g^{(2)}(t)$ and corresponding fits (*solid curves*) taken at respectively, 624, 1270, 1430, 1590, 1930, 2610 and 3230 seconds (*from left to right*) after addition of thrombin (130 pM) to a sample containing fibrinogen (150 nM), Lys^{78}-plasminogen (50 nM) and Val-Leu-Lys-pNA (600 µM) in Tris buffer at 25 °C. Values in parentheses refer to final concentrations. Equations (1) and (2) for $g^{(2)}(t)$ and $g^{(1)}(t)$, respectively, were used (see Materials and methods). The experimental and fitted $g^{(1)}(t)$ was set to 1 at $t=0$

of plasmin formation, respectively (Fig. 3B). The data for turbidity (A_{474}) versus time were plotted directly as point-to-point line graphs (Fig. 8) or transformed to derivative plots reflecting the rate of change in turbidity versus time. The derivative plots were constructed in a similar way as described for plasmin above. They were used to define the onset time of sudden increase (t_i) and the time of maximal rate of decrease (t_d) in turbidity in an analogous manner as described for the light scattering data above (compare Fig. 2A).

Assay of plasmin-catalyzed degradation of ^{125}I-labeled fribrin to fragments X, Y and D during t-PA-mediated fibrinolysis

This was done as previously described (Suenson and Thorson 1988). The moieties distinguished as fragment X by SDS-polyacrylamide gel electrophoresis were of $M_r \approx 225\,000-290\,000$ as determined by supplementary gel filtration of plasmin-degraded fibrinogen on Sepharose CL 6B (Pharmacia, Uppsala, Sweden) in 50 mM Tris-HCl, 300 mM NaCl (adjusted with NaOH to pH 7.7 at 25 °C), using Dextran 2000 and high molecular weight calibration kit (M_r 158 000–669 000) from Pharmacia (Suenson et al. 1990).

Results

Determination of the molecular mass and the diffusion coefficient for fibrinogen by dynamic light scattering

The autocorrelation function for 150 nM fibrinogen, pH 7.5, ionic strength 0.15 and temperature 25 °C has been measured and analyzed with a least squares fit using

Eqs. (1) and (2) ($\beta = 1$). The results (mean $\pm$ SEM ($n = 5$)) were a diffusion coefficient equal to $(0.21 \pm 0.01) \cdot 10^{-10}$ $m^2\ s^{-1}$ (corrected to 20 °C) and a $M_r = 332\,000 \pm 30\,000$.

Dynamic light scattering spectra from fibrin monomer assembly in the absence of t-PA

Autocorrelation functions were measured immediately after addition of 130 pM thrombin to a sample containing fibrinogen (150 nM), Lys^{78}-plasminogen (50 nM) and Val-Leu-Lys-pNA (600 μM) in Tris buffer at 25 °C. Values in parentheses refer to final concentrations. Examples of fits to the autocorrelation function during various stages of polymerization after addition of thrombin are shown in Fig. 3. In the gel phase the parameter β is significantly lower than 1, typically about 0.7. The maximal value of the length parameter L in the gel phase derived from these fits (as described in the Materials and Methods section) is about 28 μm (610 times the value for fibrinogen). The maximal value for the mass per length in the gel phase is about 100 times the value for fibrinogen (at ionic strength 0.15 M and pH 7.7).

Estimate of the form factor for fully polymerized fibrin

The autocorrelation functions were measured at 6 different angles (30°, 45°, 60°, 75°, 90° and 105°) for one fully polymerized sample of fibrin 1 h after addition of thrombin. No time effect was observed when the measurements at the six angles were repeated within one hour. The data were analyzed with a least squares fit using Eqs. (1) and (2). The ratio between the value of the form factor at 30° and 105° (mean $\pm$ SEM ($n = 10$)) was estimated, using Eq. (4), as the ratio between the apparent weight average molar mass at $\theta = 30°$ and $\theta = 105°$ and was found to be 8 ± 2. For comparison a cylinder model fit to the values of the apparent molar mass at 90° predicts a ratio of 3.6 between 30° and 105°. The average diffusion coefficient varied from $1.1 \cdot 10^{-13}$ $m^2\ s^{-1}$ at 105° to $5.8 \cdot 10^{-14}$ $m^2\ s^{-1}$ at 30°. The polydispersity was determined to be 0.4 ($\beta = 0.7$) independent of angle.

The discrepancy between the measured and calculated angular variation gives an indication of the limitation of the cylinder model in the gel phase. However, in a recent work (Farge and Maggs 1993) a theory was developed to describe the autocorrelation function of semiflexible polymers. They relate the autocorrelation function to the bending elasticity of a filament of the polymer and this to the persistence length of the filament. For the relaxation times observed here (See Fig. 3) and for the low concentration of fibrinogen used Farge and Maggs (1993) predict that

$$g_1(t) = e^{-Aq^2 t^{3/4}}$$

where a is constant which scales with $\xi^{-1/4}$. Our β value of 0.7 is in agreement with the time exponent of 3/4 and furthermore the ratio between the diffusion coefficient at 30° and that at 105° is consistent with a q^2 dependency in the exponent of the first term in Eq. (2). From the theory of Farge and Maggs it follows that our length values are likely to represent a persistence length for the linear strands in the fibrin network.

Fibrin monomer assembly and plasmin-catalyzed fibrin fragmentation studied by laser light scattering

Figure 4 shows representative progress curves of length and mass per length of fibers in the course of simultaneous fibrin monomer assembly and fibrin degradation at different concentrations of single-chain t-PA (3–100 pM). The progress curves can be divided into 3 phases, namely the first phase with a slow rate of fibrin polymerization, the second phase with a rapid rate of fibrin polymerization and the third phase dominated by fibrin fragmentation.

During the first phase (ending after 700–1500 s), it is necessary to correct for unmodified fibrinogen since it is present in significant amounts. When this correction is performed as outlined in Materials and Methods progress curves for the length and mass per length of fibrin fibers are obtained as shown in Fig. 5. It is noticed that objects with an average mass per length ratio of 2.5 relative to fibrinogen are formed right from the beginning and that molar mass changes during the first phase are due mainly to an increase in fiber length to an average value of about 10 times the length of fibrinogen. These results indicate that formation of short protofibrils dominates the first phase.

The second phase sets in after about 700 s to 1500 s, the longest delays, being observed at low t-PA concentrations (Fig. 6). This phase is characterized by sudden increase in both fiber length and mass per fiber length (lateral aggregation) to maximum values which depend on the t-PA concentration (Fig. 4). From 3 to 25 pM t-PA, the maximal length (average of 3 experiments) decreases from about 590 to about 320 and the maximal mass per length (average of 3 experiments) from about 200 to about 80 relative to fibrinogen. The curves of length divided by mass per length versus time in Fig. 5 show that the length increases more rapidly than mass per length (first peak at 3–25 pM t-PA).

The third phase dominated by fibrin fragmentation is characterized by a decrease in both length and mass per length, where the length reaches values less than 10 times the value of fibrinogen and the mass per length gets close to the value of fibrinogen (Fig. 4). The decrease in mass per length sets in earlier than the decrease in length. This is evident from the curves reflecting length divided by mass per length (Fig. 4, second peak at 3–25 pM t-PA) and from the difference between the time of the maximal rate of decrease of length and the time of the maximal rate of decrease of mass per length (Fig. 6).

Fibrin monomer assembly and plasmin-catalyzed fibrin fragmentation studied by cryo transmission electron microscopy

Figure 7 shows electron microscopy pictures of the time sequence of changes in fiber structure under the condi-

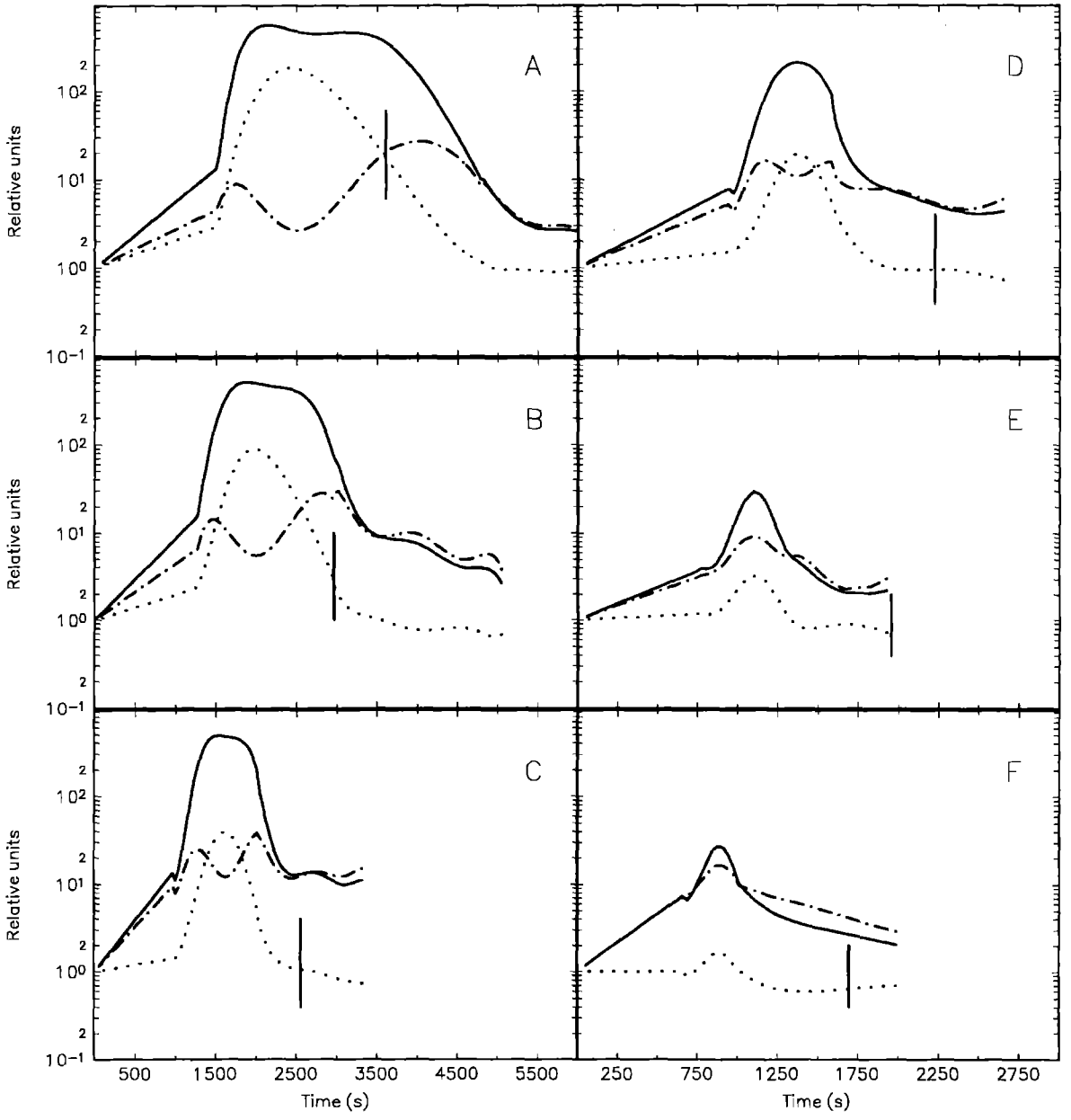

Fig. 4 A–F. Progress curves of relative length and relative mass per length of fibrin fibers during thrombin induced polymerization and single-chain t-PA-mediated fibrinolysis. Shown are the polynomial fits to the logarithm of the light scattering data (not shown) versus time for the length (*solid line*), mass per length (*dotted line*) and the length curve divided by the mass per length curve (*dot dashed line*). The data for relative length and relative mass per length were obtained via the cylinder model and fitting of the autocorrelation functions using Eqs. (1) and (2) throughout the time course. The units and the assay conditions are the same as in Fig. 2. The vertical lines indicate the times of cessation of plasmin formation. These times were equal to the t_d for mass per length + the median value (715 s) for (t_c (plasmin)$-t_d$(turbidity)) from all data in Table 1. The concentration of t-PA was 3 **A**, 6 **B**, 13 **C**, 25 **D**, 50 **E** and 100 pM **F**

tions of 13 pM t-PA used in the laser light scattering study (Compare with Fig. 5C). The specimen examined 915 sec. after initiation of the fibrin polymerization reaction revealed many small fibrin oligomers and a single relatively thick, but very long, fibrin fiber (Fig. 7A). Extensive lateral aggregation is observed after 1780 s (Fig. 7B) and evident signs of plasmin induced fragmentation is seen after 2600 s and 3600 s (Fig. 7C, D). It is noticed that plasmin degrades the fibers from within, resulting in conversion of the fibrin fibers into long loose bundles (Fig. 7C). Later they disintegrate into thin filaments (Fig. 7D). Figure 7B to 7D show branching of fibers, a feature which cannot be derived from the light scattering measurements. Otherwise the fibrin structures observed by electron microscopy are in good agreement with the laser light scattering data.

Correlation of the rate of plasmin formation to structural changes of fibrin during t-PA mediated fibrinolysis

Figure 8 shows the time courses of plasmin formation, gel turbidity and fibrin degradation during fibrinolysis in-

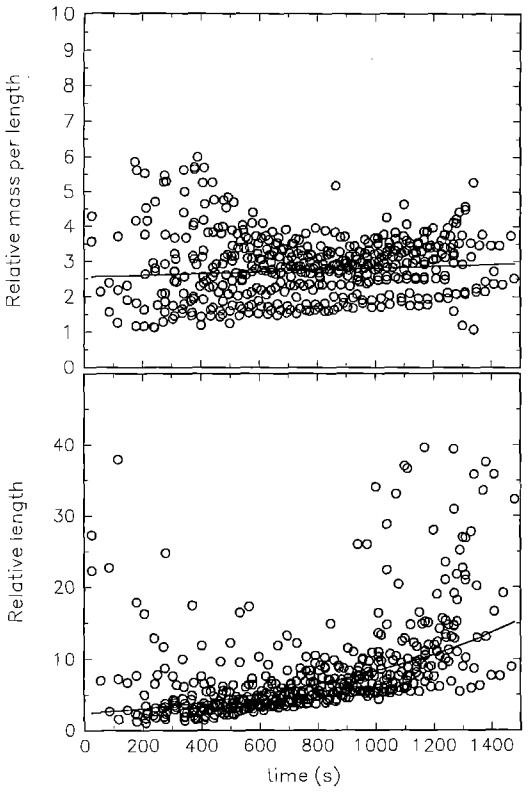

Fig. 5. The time course of length and mass per length relative to fibrinogen in the slow first phase of fibrin polymerization during single-chain t-PA-mediated fibrinolysis, after correction for the presence of fibrinogen using Eq. (1) for $g^{(2)}(t)$ and Eq. (11) for $g^{(1)}(t)$. Shown are data both without and with t-PA at 3, 6, 13, 25, 50 and 100 pM. A first order polynomial fit was made to the logarithm of the values for the length (*solid lower curve*) and mass per length (*solid upper curve*) versus time. The correction of the length and mass per length of fibrin oligomers for the presence of fibrinogen was based on the assumptions that the thrombin-catalyzed release of fibrinopeptide-A was a first order reaction with a half-life of 980 s. Data with relative length larger than 40 and mass per length larger than 6 and less than 1 were excluded

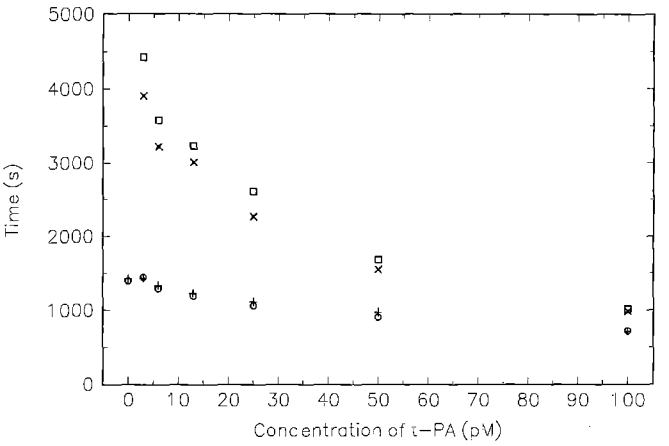

Fig. 6. Onset times (t_i) of sudden increase in length (*circles*) and mass per length (plus) and times (t_d) of maximal rate of decrease in length (*squares*) and mass per length (*crosses*) during single-chain t-PA-mediated fibrinolysis. The data are from the experiments of Fig. 4 and other similar experiments. The t_i(length) and t_i(mass per length) are defined as the intercept between the time axis and the tangent at the half maximum point before the maximum of derivative plots (Fig. 2 A) of the progress curves of length and mass per length, respectively. The t_d(length) and t_d(mass per length) are defined as the time of the minimum of derivative plots (Fig. 2 A) of the progress curves of length and mass per length, respectively. Least squares regression analysis showed a significant shortening of t_i for both length ($r=-0.875$; $P<0.001$; $n=18$) and mass($r=-0.881$; $P<0.001$; $n=18$) with increasing t-PA concentration. Non-parametric Sign Test analysis using Minitab Statistical Software, version 8.0 (Minitab Inc., PA, USA) showed that the difference, t_i(length)–t_i(mass per length) ranging between −150 s and 40, was insignificant ($P=0.48$). An average time difference between t_d(length) and t_d(mass per length) of 288 ± 76 s was determined

duced by 6 and 50 pM single-chain t-PA under conditions identical to those used for measurements of laser light scattering spectra. It is noticed that at both activator concentrations plasmin generation sets in after a lag phase, at the time where significant amounts of fibrin(ogen) starts to be converted to fragment X (compare upper and lower panels of Fig. 8). Maximal rates of plasmin formation are achieved when most of the fibrin is converted to fragment X. We ruled out the possibility that the increase in rate of plasmin formation could be related to conversion of single chain t-PA to its two-chain form. In agreement with the results obtained by others (Norrman et al. 1985; Petersen et al. 1988), identical rates of plasmin formation versus time were found with single-chain and two-chain t-PA, when analyzed at 6 or 100 pM activator (not shown). The maximal rate of plasmin formation per mol t-PA did not vary significantly with activator concentration. In experiments with single chain t-PA it was $0.027\pm0.005\ s^{-1}$, when analyzed at 3, 6, 13, 25, 50 and 100 pM activator (mean ± SEM, $n=4$ for each activator concentration). The maximal values were estimated from derivative plots reflecting the rate of plasmin formation per mol t-PA versus time. These derivative plots (an example is shown in Fig. 2 B) were constructed from data showing the amount of plasmin generated per mol t-PA versus time (Experiments of Fig. 8 and other similar experiments) as described in Materials and Methods. The stimulation of plasminogen activation ceases when substantial amounts of fragment X are converted to Y- and D-fragments (Fig. 8).

The main purpose of this study was to correlate the time course of plasmin formation with the structural changes of fibrin when analyzed by laser light scattering. A precise correlation was impeded by the fact that the data on plasmin formation (Fig. 8) and the light scattering data (Fig. 4) were obtained by analysis of separate reaction mixtures. The problem was in part circumvented by the simultaneous measurements of turbidity and plasmin formation in the same reaction mixtures and by the use of the turbidity measurements as a link to the light scattering data. The validity of this approach was based on the fact that turbidity reflects mainly mass per length of fibers (lateral aggregation) (Carr and Hermans 1978). A comparison of the time courses of plasmin generation and turbidity shows that plasmin formation sets in just prior to the sudden increase in turbidity at 50 and 100 pM t-PA (4 out of 6 experiments), while it sets in shortly after the time of the sudden increase in turbidity in most experi-

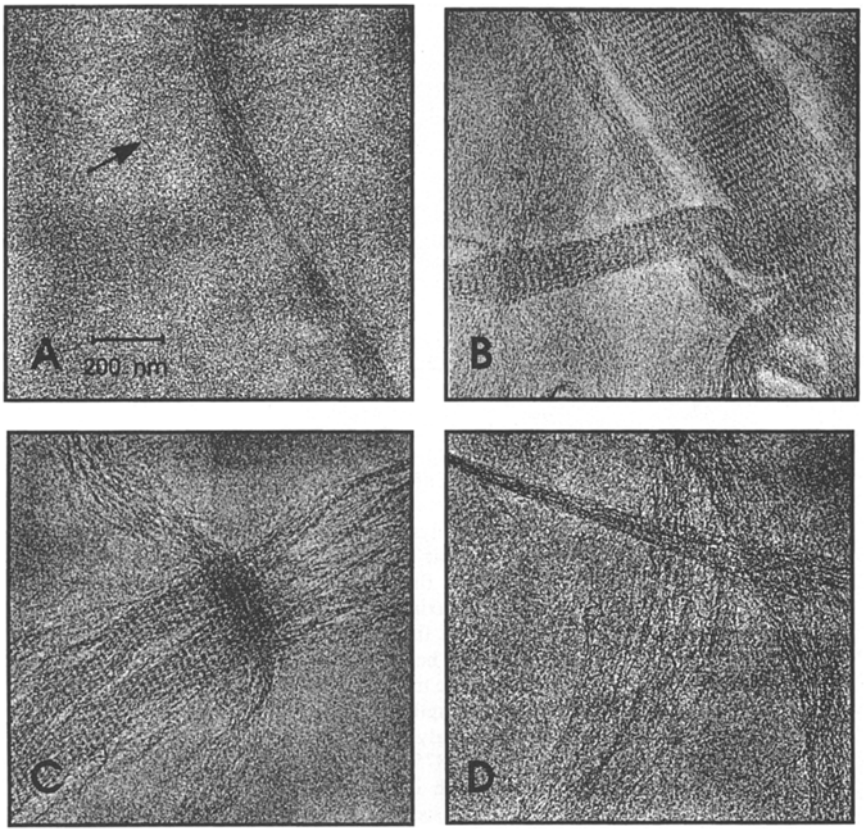

Fig. 7 A–D. Cryo transmission electron microscopy of fibrin fibers during t-PA-mediated fibrinolysis. Fibrinogen (150 nM), Lys^{78}-plasminogen (50 nM) and Val-Leu-Lys-pNA (600 μM) in Tris buffer were incubated at 25 °C. Fibrin formation and plasminogen activation were initiated by simultaneous addition of thrombin (130 mM) and t-PA (12.5 pM) in the same buffer. Values in parentheses refer to final concentrations. Specimens for electron microscopy were taken 915 s **A**, 1780 s **B**, 2600 s **C** and 3600 s **D** after addition of thrombin and t-PA. Turbidity measurements performed on the same sample which was used for cryo electron microscopy gave a time of 1230 s for the half maximal value of turbidity before the increase in turbidity and a time of 3280 s for the half maximal value of turbidity after the decline in turbidity

Table 1. Onset time (t_i(plasmin)) and cessation time of plasmin generation (t_c(plasmin)) related to onset time of sudden increase in turbidity (t_i(turbidity) and maximal rate of decrease in turbidity (t_d(turbidity)), respectively, during fibrinolysis induced by single-chain t-PA

t-PA conc. (pM)	(t_i(plasmin)–t_i(turbidity)) (s)	n	(t_c(plasmin)–t_d(turbidity)) (s)	n
3	480 (230–680)	4		
6	225 (100–490)	6	1020 (940–1100)	2
13	125 (50–200)	4	400	1
25	20 (−440–90)	4	660 (480–860)	3
50	−25 (−390–100)	6	785 (420–970)	6
100	−140 (−280–10)	4	675 (630–790)	4

The data [median (range)] are derived from the experiments of Fig. 8 (*upper and middle panels*) and other similar experiments. The t_i(plasmin) and t_c(plasmin) are defined as the intercept between the time axis and the tangent at the half maximum before and after the maximum of derivative plots reflecting the rate of plasmin formation versus time (Fig. 3 B). The t_i(turbidity) and t_d(turbidity) are defined in the same way as the analogous parameters for length and mass per length, respectively. (See legends to Tables 1 and 2)

ments at lower activator concentrations (Fig. 8 and Table 1). Assuming, that the onset times of sudden increases in turbidity (Fig. 8) and in mass per length of fibrin fibers (Fig. 4) are comparable, it can be inferred that plasmin formation at the high t-PA concentrations sets in at the stage where short protofibrils are present (Fig. 5), while at the low t-PA concentrations plasmin formation sets in after the onset of lateral aggregation (Fig. 4).

Plasmin generation ceases 715 s (median value) after the time of maximal rate of decrease in turbidity at all concentrations of activator (Table 1). Assuming that the maximal decrease in the rate of turbidity reflects the maximal rate of decrease in mass per length it can be inferred that the mass per length of fibrin fibers at cessation of stimulation of plasminogen activation is about the same as that of fibrinogen at all concentrations but 3 pM of t-PA and that the length decreases from about 300 to about 3 times that of fibrinogen when the t-PA concentration is increased from 3 to 100 pM (Fig. 4).

Discussion

In the present study fibrin structures were related to the stimulatory effect of fibrin on plasminogen activation during t-PA-mediated fibrinolysis. Structural studies were undertaken by analysis of static and dynamic laser light scattering spectra, cryo transmission electron microscopy and by analysis of plasmin-cleavage of fibrin to X-, Y- and D-fragments. The stimulatory effect of fibrin was analyzed by measurement of the time course of plasmin formation. Very low concentrations of thrombin (130 pM) and t-PA (3–100 pM) were used to initiate fibrin formation and fibrin degradation, respectively. At these low concentrations the proteolytic processes were slowed down sufficiently to enable the characterization of fibrin structures in the course of the reciprocal improvement of fibrin stimulation of plasminogen activation and the plasmin-cleavage of the fibrin.

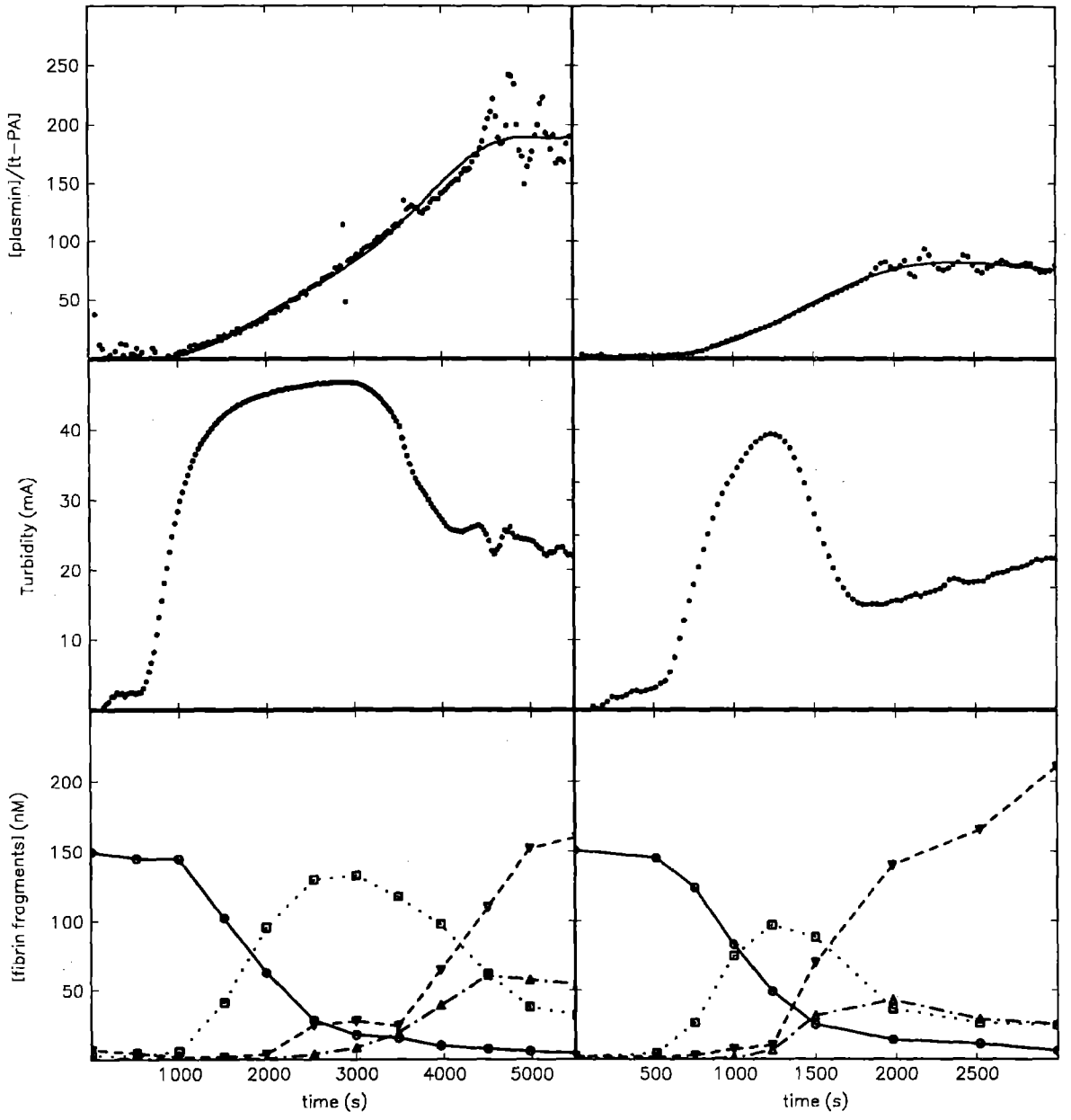

Fig. 8. Progress curves of plasmin formation, fibrin polymer turbidity and plasmin degradation of ^{125}I-labeled fibrin during single-chain t-PA mediated fibrinolysis. Fibrinogen (150 nM), Lys^{78}-plasminogen (50 nM) and Val-Leu-Lys-pNA (600 μM) in Tris buffer were incubated at 25 °C in a thermostated cuvette. Fibrin formation and plasminogen activation were initiated by simultaneous addition of thrombin (130 pM) and t-PA 6 pM (*left panels*) or 50 pM (*right panels*) in the same buffer. Values in parentheses refer to final concentrations. Plasmin concentrations (*upper panels*) and fibrin turbidity (*middle panels*) were monitoring continuously and simultaneously in the same reaction mixtures. Plasmin concentrations were calculated from the rate of release of pNA as described in Materials and methods. Plasmin degradation of ^{125}I-labeled fibrin (*lower panels*) was monitored in separate reaction mixtures. ^{125}I-Labeled fibrin (●), fragments X (■), Y (▲) and D (▼) were quantified as described in Materials and methods

The process of fibrin polymerization and fibrin degradation can be divided into 3 phases. During the entire first phase (ending after 700–1500 s) the average mass per length of fibers was about 2.5–3 times that of fibrinogen, while the average fiber length increased to a value of about 10 times the length of fibrinogen (Fig. 5). This is consistent with the results obtained by others that the first phase of fibrin polymerization is governed by formation of short oligomeric protofibril structures, resulting from self-association of desA-fibrin monomers or association of desA-fibrin monomers and fibrinogen (Jamney et al. 1983; Hantgan et al. 1983; Lewis et al. 1985; Medved' et al. 1990; Shainoff and Dardik 1983; Wilf and Minton 1986; Wolfe and Waugh 1981; Weisel and Nagaswami 1992). The second phase of fibrin polymerization and fibrin degradation was characterized by a sudden increase in both fiber length and mass per length (lateral aggregation) of fibers (Fig. 4). This sudden change in rate of fibrin polymerization is compatible with the results obtained by others and conforms with the fact that protofibrils have to reach a certain length before lateral aggregation of fibers takes place (Janmey et al. 1983; Hantgan and Hermans

1979; Hantgan et al. 1993; Medved' et al. 1990; Wilf and Minton 1986; Wolfe and Waugh 1981; Weisel and Nagaswami 1992).

The value of the length parameter L in the gel phase derived from the cylinder model fits (as described in the Materials and Methods section) is in the range of 10 to 50 μm and does not represent a true length of the fibers (this is true for the gel state, independent of the t-PA concentration) but rather an equivalent length of a rigid cylinder. The relationship between the structure of a gel and its scattering and hydrodynamic properties has not been worked out. However, as shown by Carr and Hermans (1978) the scattering at 90° follows the behavior of elongated rods even in the gel state. The mass per unit length obtained from gel permeation, light scattering and turbidimetry (Carr et al. 1977; Carr and Hermans 1978) at the concentration of fibrinogen used here was 130 times the value for fibrinogen (assuming a value of 7400 Daltons per nM for fibrinogen) at ionic strength = 0.15 M and pH 7.4. When no t-PA is present the maximal value of about 100 for the mass per length in the gel phase (at ionic strength 0.5 M and pH 7.7) is in good agreement with the above cited value of 130.

As stated in the results section the maximal values achieved for length and mass per length of fibrin fibers decrease with increasing t-PA concentration (Fig. 4) resulting from a higher rate of plasmin formation and a higher rate of conversion of fibrin to fragment X (Fig. 8). This is consistent with the fact that early plasmin-cleavages of fibrin in both the NH_2-terminal(B)β-chains and in the COOH-terminal (A)α-chains in the course of fragment X formation impair fibrin polymerization sites (Medved' et al. 1986; Shen et al. 1977; Siebenlist et al. 1990). The third phase of fibrin polymerization and degradation was characterized by extensive plasmin-cleavage reducing fiber length to less than 10 times the length of fibrinogen and fiber thickness to values close to the value obtained for fibrinogen. Fiber length decreased later than the fiber thickness (Figs. 4 and 6) indicating that the fibers primarily dissociated into long thin bundles. This agrees with cryo electron microscopy of specimens which showed that plasmin degraded fibrin fibers from within, resulting in conversion of the fibers into long loose bundles (Fig. 7C). Later, the loose bundles disintegrate into thin filaments (Fig. 7D). During the third phase fragment X was converted to fragments Y and D (Fig. 8).

Significant formation of plasmin was found to set in close to the onset time of the sudden increase in turbidity (Fig. 8 and Table 1). In most experiments at 50 and 100 pM t-PA, the onset time of plasmin generation preceded the onset time of the sudden increase in turbidity, while at concentrations less than 50 pM t-PA the onset time of plasmin generation sets in after the time of the sudden increase in turbidity. Assuming, that the onset times of sudden increases in turbidity (Fig. 8) and in mass per length of fibrin fibers (Fig. 4) are comparable (Carr and Hermans 1978), it can be inferred that plasmin formation at the high t-PA concentrations sets in at the stage where short protofibrils with a length of about 10 times that of fibrinogen dominate (Fig. 5), while plasmin formation at the low t-PA concentrations sets in after the onset of lateral aggregation (Fig. 4). The onset of plasmin formation after the onset of lateral aggregation at the low-PA concentrations was associated with a later onset of the stage where the maximal rate of plasmin formation was achieved (Fig. 8). This was most likely related to the slower rate of generation of fragment X-polymer at the low than at the hight concentrations of t-PA and to the correspondence between the amount of fragment X and the rate of plasminogen activation (Suenson et al. 1990). Approximately the same value for the maximal rate of plasmin formation per mol t-PA ($=k_{cat}/(1+K_m/[Lys^{78}\text{-plasminogen}])$) was attained at all concentrations of activator (see results section). This value agrees with that which can be calculated from the reported kinetic data on activation of Lys^{78}-plasminogen by t-PA in the presence of fragment X-polymer (Suensen et al. 1990). Plasmin formation ceased 400–1020 s after the time of the maximal rate of decrease of turbidity (Table 1), which was assumed to be comparable with the maximal rate of decrease of mass per length. At this stage, the mass per length of fibers was about the same as that of fibrinogen (except at 3 pM t-PA) and the length ranged from about 300 to about 3 relative to fibrinogen, the longest fibers being formed at the low activator concentrations (Fig. 4). The cessation of plasmin formation was correlated with extensive degradation of fragment X to fragments Y and D, confirming the results of Suenson et al. (1984, 1990).

Both the D- and the E-region of fibrinogen have been reported to contain binding sites for t-PA (Bosma et al. 1988; Hasan et al. 1992; Weitz et al. 1991) and plasminogen (Bosma et al. 1988; Váradi and Patthy 1983, 1984; Wiman et al. 1979). In addition a t-PA binding site has been located in the coiled coil region of the Aα(148–160)-chain (Yonekawa et al. 1992). These binding sites appear to be masked in intact fibrinogen, but to be exposed during thrombin and plasmin modification of the fibrinogen molecule. It has been reported that soluble (DD)E complex is an effective stimulator of plasminogen activation (Hasan et al. 1992; Weitz et al. 1991). It is very likely that the DDE regions of the fragment X protofibrils play a decisive role for the binding of t-PA and plasminogen and the subsequent optimal stimulation of plasminogen activation.

In agreement with the results reported by Gaffney et al. (1983), the onset time of the sudden increase of fibrin assembly shortened with increasing concentration of t-PA (Fig. 1). This may be explained by the recent observation that t-PA can catalyze the release of fibrinopeptides A and B from fibrinogen, fibrinopeptide B being cleaved off at the highest rate (Weitz et al. 1988). Another possibility may be that very early plasmin-cleavage of fibrin protofibrils increased the rate of lateral aggregation of protofibrils. It has been demonstrated that under certain conditions the rate of fragment-X polymerization is higher than the rate of fibrin polymerization (Sato and Weisel 1990).

In conclusion our results indicate that (1) formation of short fibrin protofibrils is the minimal requirement for the onset of the stimulatory effect of fibrin on plasminogen activation by t-PA, (2) formation of fragment X protofibrils is sufficient to induce optimal stimulation of

plasminogen activation, and (3) plasmin degrades laterally aggregated fibrin fibers from within resulting in the conversion of the fibers into long loose bundles, which later disintegrate into thin filaments.

Acknowledgements. Excellent laboratory assistance from Katja Brodersen, Birgitte Korsholm and Birgitte Lillethorup is gratefully acknowledged.

References

Blombäck B, Okada M (1982) Fibrin gel structure and clotting time. Thromb Res 25:51–70

Bosma PJ, Rijken DC, Nieuwenhuizen W (1988) Binding of tissue-type plasminogen activator to fibrinogen fragments. Eur J Biochem 172:339–404

Carr MC Jr, Shen LL, Hermans J (1977) Mass length ratio of fibrin fibers from gel permeation and light scattering. Biopolymers 16:1–15

Carr MC, Herman J (1978) Size and density of fibrin fibers from turbidity. Macromolecules 11:46–50

Casassa EF (1955) Light scattering from very long rod-like particles and an application to polymerized fibrinogen. J Chem Phys 23:596–597

Doolittle RF (1984) Fibrinogen and fibrin. Ann Rev Biochem 53:195–229

Farge E, Maggs AC (1993) Dynamic scattering from semiflexible polymers. Macromolecules 26:5041–5044

Feigin LA, Svergun DI (1987) Structure Analysis by Small-angle X-ray and Neutron Scattering. Plenum Press, New York

Forsgren M, Råden B, Israelsson M, Larsson K, Hedén L-O (1987) Molecular cloning and characterization of full-length cDNA clone for human plasminogen. FEBS Lett 213:254–260

Gaffney PJ, Templeman J, Mahmoud M, Perry MJ (1983) Fibrin formation: The influence of plasminogen, thrombin and calcium. Thromb Haemostas 50:355 (Abstract no. 1117)

Hantgan RR, Hermans J (1979) Assembly of fibrin, a light scattering study. J Biol Chem 254:11272–11281

Hantgan RR, McDonagh J, Hermans J (1983) Fibrin assembly. Ann NY Acad Sci, USA 408:345–366

Hasan AAK, Chang WS, Budzynski AZ (1992) Binding of fibrin fragments to one-chain and two-chain tissue-type plasminogen activator. Blood 79:2313–2321

Hoylaerts M, Rijken DC, Lijnen HR, Collen D (1982) Kinetics of the activation of plasminogen by human tissue plasminogen activator. Role of fibrin. J Biol Chem 257:2912–2919

Hunziker EB, Straub PW, Haeberli A (1990) A new concept of fibrin formation based upon the linear growth of interlacing and branching polymers and molecular alignment into interlocked single-stranded segments. J Biol Chem 265:7455–7463

Janmey PA, Erdile L, Bale MD, Ferry JD (1983) Kinetics of fibrin oligomer formation observed by electron microscopy. Biochemistry 22:4336–4340

Jørgensen M, Petersen LC, Thorsen S (1984) Purification and characterization of hereditary anbormal antithrombin III with impaired thrombin binding. J Lab Clin Med 104:245–256

Kaczmarek E, Lee MH, McDonagh J (1993) Initial interaction between fibrin and tissue plasminogen activator (t-PA). The Gly-Pro-Arg-Pro binding site on fibrin(ogen) is important for t-PA activity. J Biol Chem 268:2474–2479

Lewis SD, Shields PP, Shafer JA (1985) Characterization of the kinetic pathway for liberation of fibrinopeptides during assembly of fibrin. J Biol Chem 260:10192–10199

Maguire JF (1981) Rotational dynamics of rigid rods. J Chem Soc Faraday Trans 77:513–518

Marx G (1988) Mechanism of fibrin coagulation based on selective, cation-driven, protofibril association. Biopolymers 27:763–774

Medved LV, Gorkum OV, Manyakov VF, Belitser VA (1986) αC-Domains of fibrinogen as a structure accelerating the autoassembly of fibrin. Molekulyarnaya Biologiya 20:461–470. English translation: Plenum Press, New York

Medved L, Ugarova T, Veklich Y, Lukinova N, Weisel J (1990) Electron microscope investigation of the early stages of fibrin assembly. J Mol Biol 216:503–509

Mihalyi E (1983) Kinetics and molecular mechanism of the proteolytic fragmentation of fibrinogen. Ann NY Acad Sci, USA 408:60–70

Montejo JM, Razi Naqvi K, Pilar Lillo M, Gonzalez-Rodriguez J, Ulises Acuna A (1992) Conformation of human fibrinogen in solution from polarized triplet spectroscopy. Biochemistry 31:7580–7586

Mosseson MW (1992) The role of fibrinogen and fibrin in hemostasis and thrombosis. Sem Hematol 29:177–188

Mueller M, Burchard W (1978) Fibrinogen-fibrin transformations characterized during the course of reaction by their intermediate structure. Biochim Biophys Acta 537:208–225

Norrman B, Wallén P. Rånby M (1985) Fibrinolysis mediated by tissue plasminogen activator. Disclosure of a kinetic transition. Eur J Biochem 149:193–200

Nossel HL, Hurlet-Jensen A, Liu CY, Koehn JA, Canfield RE (1983) Fibrinopeptide release from fibrinogen. Ann NY Acad Sci, USA 408:269–278

Palmer GR, Fritz OG, Hallett FR (1979) Quasielastic light-scattering studies on human fibrinogen and fibrin. I. Fibrinogen. Biopolymers 18:1647–1658

Palmer GR, Fritz OG, Hallett FR (1979) Quasielastic light-scattering studies on human fibrinogen and fibrin. II. Fibrinogen. Biopolymers 18:1659–1672

Patterson GD (1983) Photon correlation spectroscopy of bulk polymers. Adv Polymer Sci 148:125–159

Petersen LC, Handest P, Brender J, Selmer J, Jørgensen M, Thorsen S (1987) A sensitive solid-phase immunosorbent assay for tissue-type plasminogen activator activity in plasma using trinitrobenzoylated poly-D-lysine as stimulator of plasminogen activation. Thromb Haemostas 57:205–211

Petersen LC, Johannessen M, Foster D, Kumar A, Mulvihill E (1988) The effect of polymerised fibrin on the catalytic activities of one-chain tissue-type plasminogen activator as revealed by an analogue resistant to plasmin cleavage. Biochim Biophys Acta 952:245–254

Provencher SW (1982) A constrained regularization method for inverting data represented by linear algebraic or integral equations. Comput Phys Commun 27:213–227

Richards EG (1980) An Introduction to Physical Properties of Large Molecules in Solution. Cambridge University Press, Cambridge

Russo PS (1993) Dynamic light scattering from rigid and nearly rigid rods in Dynamic light scattering. The method and some application. Brown W (ed) Clarendon Press, Oxford, pp 512–554

Sato H, Weisel JW (1990) Polymerization of fibrinogen-derived fragment X and subsequent rearrangement of fibers. Thromb Res 58:205–212

Schmitz KS (1990) Dynamic Light Scattering by Macromolecules. Academic Press, New York

Shafer JA, Higgins DL (1988) Human fibrinogen. CRC Crit Rev Lab Sci 26:1–41

Shainoff JR, Dardik BN (1983) Fibrinopeptide B in fibrin assembly and metabolism: Physiologic significance in delayed release of the peptide. An NY Acad Sci, USA 408:255–268

Shen LL, McDonagh RP, McDonagh J, Hermans J (1977) Early events in the plasmin digestion of fibrinogen and fibrin. Effects of plasmin on fibrin polymerization. J Biol Chem 252:6184–6189

Siebenlist KR, DiOrio JP, Budzynski AZ, Mosesson MW (1990) The polymerization and thrombin-binding properties of des-(Bβ1-42)-fibrin. J Biol Chem 265:18650–18655

Suenson E, Petersen LC (1986) Fibrin and plasminogen structures essential to stimulation of plasmin formation by tissue-type plasminogen activator. Biochim Biophys Acta 870:510–519

Suenson E, Thorsen S (1988) The course and prerequisites of Lys-plasminogen formation during fibrinolysis. Biochemistry 27:2435–2443

Suenson E, Lützen O, Thorsen S (1984) Initial plasmin-degradation of fibrin as the basis of a positive feed-back mechanism in fibrinolysis. Eur J Biochem 140:513–522

Suenson E, Bjerrum P, Holm A, Lind B, Meldal M, Petersen LC, Selmer J (1990) The role of fragment X polymers in the fibrin enhancement of tissue plasminogen activator-catalyzed plasmin formation. J Biol Chem 265:22228–22237

Thorsen S (1975) Differences in the binding to fibrin of native plasminogen and plasminogen modified by proteolytic degradation. Influence of ω-aminocarboxylic acids. Biochim Biophys Acta 393:55–65

Thorsen S (1992) The mechanism of plasminogen activation and the variability of the fibrin effector during tissue-type plasminogen activator-mediated fibrinolysis. Ann NY Acad Sci, USA 667:52–63

Van der Drift ACM, Poppema A, Haverkate F, Nieuwenhuizen W (1983) In: Fibrinogen. Structure, Functional Aspects, Metabolism. (Haverkate F, Henschen A, Nieuwenhuizen W, Straw PW (eds) Walter de Gruyter, Berlin, p 3

Váradi A, Patthy L (1983) Location of plasminogen-binding sites in human fibrin(ogen). Biochemistry 22:2440–2446

Váradi A, Patthy L (1984) $\beta(Leu_{121}–Lys_{122})$ Segment of fibrinogen is in a region essential for plasminogen binding by fibrin fragment E. Biochemistry 23:2108–2112

Wachenfeld-Eisele E, Burchard W (1988) Cured epoxy resins: Measurements in dilute and semidilute solutions in biological and synthetic polymer networks in Biological and Synthetic Polymer Networks. Kramer O (ed) Elsevier, London, New York, p 305–319

Weisel JW, Nagaswami C (1992) Computer modeling of fibrin polymerization kinetics correlated with electron microscope and turbidity observations: Clot structure and assembly are kinetically controlled. Biophys J 63:111–128

Weitz JI, Cruickshank MK, Thong B, Leslie B, Levine MN, Ginsberg J, Eckhardt T (1988) Human tissue-type plasminogen activator releases fibrinopeptides A and B from fibrinogen. J Clin Invest 82:1700–1707

Weitz JI, Leslie B, Levine MN, Ginsberg J (1991) Soluble fibrin degradation products potentiate tissue plasminogen activator-induced fibrinogen proteolysis. J Clin Invest 87:1082–1090

Wilf J, Minton AP (1986) Soluble fibrin-fibrinogen complexes as intermediates in fibrin gel formation. Biochemistry 25:3124–3133

Wiltzius P, Känzig W, Häberli A, Straub PW (1982) Fibrin polymerization studied by static and dynamic light-scattering as a function of fibrinopeptide A release. Biopolymers 21:2205–2223

Wiman B, Hamsten A (1990) The fibrinolytic enzyme system and its role in the etiology of thromboembolic disease. Sem Thromb Hemostas 16:207–216

Wiman B, Lijnen HR, Collen D (1979) On the specific interaction between the lysine-binding sites in plasmin and complementary sites in α_2-antiplasmin and in fibrinogen. Biochim Biophys Acta 579:142–154

Wolfe JK, Waugh DF (1981) Relations between enzymatic and association reactions in the development of bovine fibrin clot structure. Arch Biochem Biophys 221:125–142

Yonekawa O, Voskuilen M, Nieuwenhuizen W (1992) Localization in the fibrinogen gamma-chain of a new site that is involved in the acceleration of the tissue-type plasminogen activator-catalysed activation of plasminogen. Biochem J 283:187–191